



HAL
open science

Ultraspecific live imaging of the dynamics of zebrafish neutrophil granules by a histopermeable fluorogenic benzochalcone probe

Emma Colucci-Guyon, Ariane S Batista, Suellen D S Oliveira, Magali Blaud, Ismael C Bellettini, Benoit Marteyn, Karine Leblanc, Philippe Herbomel, Romain Duval

► To cite this version:

Emma Colucci-Guyon, Ariane S Batista, Suellen D S Oliveira, Magali Blaud, Ismael C Bellettini, et al.. Ultraspecific live imaging of the dynamics of zebrafish neutrophil granules by a histopermeable fluorogenic benzochalcone probe. *Chemical Science*, 2019, 10 (12), pp.3654-3670. 10.1039/c8sc05593a . hal-02359369

HAL Id: hal-02359369

<https://hal.science/hal-02359369>

Submitted on 12 Nov 2019

HAL is a multi-disciplinary open access archive for the deposit and dissemination of scientific research documents, whether they are published or not. The documents may come from teaching and research institutions in France or abroad, or from public or private research centers.

L'archive ouverte pluridisciplinaire **HAL**, est destinée au dépôt et à la diffusion de documents scientifiques de niveau recherche, publiés ou non, émanant des établissements d'enseignement et de recherche français ou étrangers, des laboratoires publics ou privés.

ARTICLE

Ultraspecific live imaging of the dynamics of zebrafish neutrophil granules by a histopermeable fluorogenic benzochalcone probe

Emma Colucci-Guyon^{1,2,*}, Ariane S. Batista^{3,1}, Suellen D. S. Oliveira^{4,1}, Magali Blaud⁵, Ismael C. Bellettini⁶, Benoit S. Marteyn^{7,8}, Karine Leblanc⁹, Philippe Herbomel^{1,2} & Romain Duval^{10,*}

Neutrophil granules (NGs) are key components of the innate immune response and mark the development of the hematopoietic system in mammals. However, no specific fluorescent vital stain existed up to now to monitor their dynamics within a whole live organism. We rationally designed a benzochalcone fluorescent probe (HAB) featuring high tissue permeability and optimal photophysics such as elevated quantum yield, pronounced solvatochromism and target-induced fluorogenesis. Phenotypic screening identified HAB as the first cell- and organelle-specific small-molecule tracer of NGs in live zebrafish larvae, with no labeling of any other cell types or organelles. HAB staining was independent of the state of neutrophil activation, labeling NGs of both resting and phagocytically-active cells with equal specificity. By high-resolution live imaging, we documented the dynamics of HAB-stained NGs during phagocytosis. Upon zymosan injection, labeled NGs were rapidly recruited to the forming phagosome in live zebrafish phagocytosing neutrophils. Despite being a reversible ligand, HAB could not be displaced by high concentrations of pharmacologically-relevant competing chalcones, indicating that this specific labeling was the result of HAB precise physicochemical signature rather than a general feature of chalcones. However, one of the competitors was discovered as a promising interstitial fluorescent tracer illuminating zebrafish histology, similarly to BODIPY-ceramide. As a yellow-emitting histopermeable vital stain, HAB functionally and spectrally complements most genetically-incorporated fluorescent tags commonly used in live zebrafish biology, holding promise for the study of neutrophil-dependent responses relevant to human physiopathology such as developmental defects, inflammation and infection. Furthermore, HAB intensely labeled isolated live human neutrophils at the level of granulated subcellular structures consistent with human NGs, suggesting that the labeling of NGs by HAB is not restricted to the zebrafish model but also relevant to mammalian systems.

¹Institut Pasteur, Unité Macrophages et Développement de l'Immunité, Paris, France. ²CNRS UMR 3738, Paris, France. ³Nanotechnology Engineering Program, Instituto Alberto Luiz Coimbra de Pós-Graduação e Pesquisa de Engenharia - COPPE, Universidade Federal do Rio de Janeiro, Rio de Janeiro, 21941-972, Brazil. ⁴Department of Anesthesiology, University of Illinois, Chicago, 60612, USA. ⁵These co-authors contributed equally to this work. ⁶LCRB, CNRS, Université Paris 5, Sorbonne Paris Cité, Paris, 75006, France. ⁷Departamento de Ciências Exatas e Educação, Universidade Federal de Santa Catarina, Blumenau, 89036-256, Brazil. ⁸Institut Pasteur, Unité de Pathogénie Microbienne Moléculaire, Paris, 75015, France. ⁹INSERM UMR 786, Paris, France. ¹⁰BioCIS, CNRS, Université Paris-Sud 11, Châtenay-Malabry, 92290, France. ¹⁰MERIT, IRD, Université Paris 5, Sorbonne Paris Cité, Paris, 75006, France. Correspondence and requests for materials should be addressed to E. C.-G. (email: emma.colucci@pasteur.fr) or to R. D. (email: romain.duval@ird.fr).

The zebrafish (*Danio rerio*), a precious vertebrate model in developmental biology, has recently emerged as a powerful non-mammalian model to study the development and the function of the immune system and to address host-pathogen interaction in the context of an entire live organism. The small size and the natural translucency of the zebrafish embryo and swimming larva make it possible to follow leukocyte deployment, behavior and functions *in vivo* at high resolution throughout the organism.^{1,2} Maturation and deployment of myeloid cell lineages have been characterized for more than a decade. The zebrafish possesses a multi-lineage myeloid compartment with two types of granulocytes (heterophil/neutrophil and eosinophil granulocytes), and monocyte/macrophages, each with characteristic morphological and histochemical features. Macrophages appears during the first day of zebrafish development, followed by neutrophils that arise a day later, both leukocytes representing together a first, efficient immune system for the developing fish.³⁻⁵ Zebrafish neutrophils are morphologically and functionally similar to their mammalian counterpart. They are equipped with granules containing microbicidal compounds, they engulf and kill invading microorganisms, and have been extensively studied for their key roles in innate immunity and inflammation. The availability of transgenic fish lines expressing GFP or other fluorescent proteins under the control of specific neutrophil promoters allows the live imaging of neutrophil behavior in the context of the entire organism.^{6,7} Although several small-molecule tracers of neutrophil granules have been described (e. g., quinacrine, LysoTrackerRed[®], fluorescent tyramide conjugates or Sudan Black staining for endogenous peroxidase containing granules), they are either non-specific in terms of labeled organelles or limited to fixed samples and therefore unusable as vital stains for live animal imaging.^{5,8,9}

In our development of fluorescent organic dyes for biological applications, we searched for small size, non-canonical fluorophores with novel structure-fluorescence relationships (SFRs)¹⁰, and identified the chalcone scaffold as such a motif. Chalcones (1,3-diphenyl-2-propen-1-ones) have been investigated as fluorescent chemosensors for several analytical applications,¹¹⁻¹³ and as pharmacological probes in a few cases.¹⁴⁻¹⁷ However, their development as fluorotracers has remained hampered by suboptimal photophysics such as minute to modest quantum yields,¹¹⁻¹³ by poor cytopermeabilities limiting biological labeling to cell surfaces^{14,15} or extracellular deposits,¹⁷ by substantial non-specific labeling,¹⁶ and by weakly documented SFRs.^{14-16,18} These constitute severe drawbacks for potential fluorophores that are otherwise compact, easy to synthesize and also spectrally tractable by chemical modulation. They define the challenges to be addressed in the design of an optimal chalcone probe for biological studies.

Results

Probe synthesis and fluorescence structure-activity relationships. Chalcone itself is intrinsically non-fluorescent. Towards emissive chalcones possessing optimal photophysics and high cytopermeability for live-cell and live-animal imaging, we rationally delineated minimal structural modifications of the 1,3-diarylpropenone system (Scheme 1). Organic fluorophores are classically composed of push-pull moieties connected by means of an extended conjugation, allowing efficient excited state intramolecular charge transfers (ICTs).¹⁰ Accordingly, an electrodonating aromatic ring (B) would be conjugated to the enone system, with the arylcarbonyl (A) acting as electron-withdrawing moiety in the chalcone system (Fig. 1). The electrodonating aryle was chosen as a naphthyle group, known to increase fluorescence intensity while exerting bathochromic effects with respect to the phenyle group.^{10, 19} This shift is useful for microscopic imaging as it diminishes light scattering, cellular auto-fluorescence and phototoxicity.^{20, 21} In addition, the more lipophilic naphthyle nucleus would dramatically increase the ability of a given probe to penetrate cells and organelles. We finally settled on a pivotal primary amino group as the electrodonating substituent, having in mind its useful transformation to the azide for fluorogenic photolabeling strategies of cells or proteomes.²² Accordingly, we targeted the 3-aminobenzochalcone core as the optimal fluorophore in this series, featuring the most extended captodative system, and expected to display maximal fluorescence intensity and bathochromism (Fig. 1).

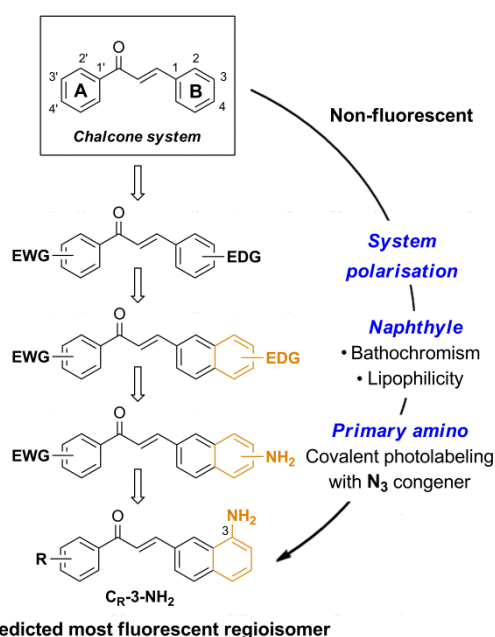


Figure 1 Stepwise design of a minimal cytopermeable chalcone fluorophore (EWG, electro-withdrawing group; EDG, electro-donating group; R, any substituent).

These 3-aminobenzochalcones were obtained by reduction of the corresponding nitro intermediates, accessed by Claisen-Schmidt condensation of various acetophenones with 8-nitro-2-naphthaldehyde **2**. Starting from β -naphthaldehyde **1**,²³ a small library of benzochalcones **3-8** was thus obtained where the electron density of the acetophenyle part was tuned from severely deficient ($R = 4'-CF_3$) to strongly enriched ($R = 4'-OH$). Two close analogues were synthesized for the physicochemical standardization of this new series: (i) 5-aminobenzochalcone **12** is a regioisomer of 3-aminobenzochalcone **8**, possessing a less extended captodative system as a pseudo-*para* conjugation; (ii) 2-aminochalcone **14** is the exact chalcone congener of 3-aminobenzochalcone **6**, and should permit to quantify the influence of the naphthyle ring both in terms of fluorescence and lipophilicity. Compound **12** was obtained from β -methylnaphthalene **9** upon regioselective nitration²⁴ then methyle oxidation. The obtained 6-nitro-2-naphthaldehyde **11** was turned to 5-aminobenzochalcone **12** by a "one-pot" condensation-reduction as for aminochalcones **3-8**. 2-aminochalcone **14** was obtained from 2-nitrobenzaldehyde **13** following the same strategy (Fig. 2a) (see Electronic Supplementary Information for all synthetic procedures).

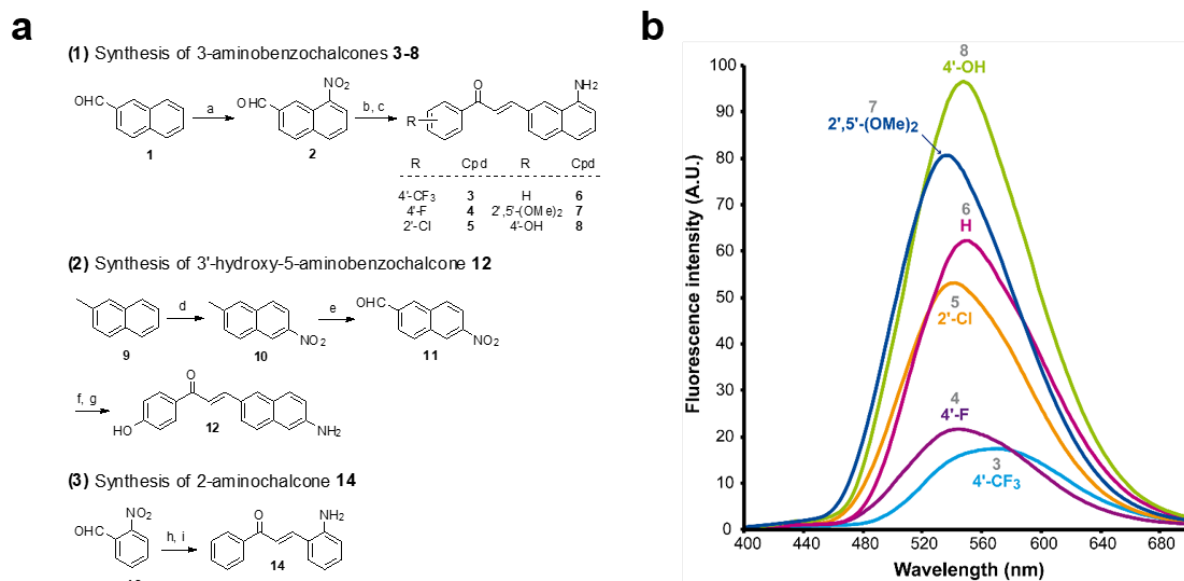


Figure 2 Synthesis of representative compounds in the 3-aminobenzochalcone, 5-aminobenzochalcone and 2-aminochalcone series and SFRs in the 3-aminobenzochalcone series. (a) Reagents and conditions: a) HNO₃ (40 equiv.), H₂SO₄ (1.5 equiv.), AcOH, r. t., 13 % **2; b) substituted acetophenone (1 equiv.), NaOH (0.75-2 equiv.), EtOH, r. t.; c) SnCl₂ (5-10 equiv.) or cat. Pd-C (10 %), H₂, AcOH, r. t., 38 % **3**, 31 % **4**, 26 % **5**, 37 % **6**, 18 % **7**, 69 % **8**; d) HNO₃ (1.25 equiv.), Ac₂O, r. t., 11 % **10**; e) SeO₂ (2 equiv.), neat, 150 °C, 28 % **11** (45 % based on conversion); f) 4-hydroxyacetophenone (1 equiv.), NaOH (2 equiv), EtOH, r. t.; g) Fe (10 equiv.), AcOH, reflux, 56 % **12**; h) acetophenone (1 equiv.), NaOH (0.75 equiv), EtOH, r. t.; i) Pd-C (10 %), H₂, AcOH, r. t., 12 % **14** (yields of chalcones indicated for two-steps, “one-pot” reactions). See Electronic Supporting Information for all synthetic procedures. (b) Semi-quantitative emission spectra of 3-aminobenzochalcones **3-8** (50 μM) in toluene at 20 °C.**

3-Aminobenzochalcones were indeed fluorescent compounds, in agreement with our design of this novel fluorophore. However, while electro-withdrawing acetophenylene rings were expected to yield the most fluorescent compounds (Scheme 1), the strongest fluorescence was associated to the electrodonating 4'-hydroxy group (cpd **8**), while a 4'-trifluoromethyl group (cpd **3**) induced a much weaker fluorescence (Fig. 2b). The spectral properties of these fluorophores are given in Table S1 in the Electronic Supplementary Information and depicted in Fig. 3. 3-Aminobenzochalcones optimally display high Stokes shifts predicting an absence of internal quenching, with emission in the green-yellow region of the visible spectrum in toluene. As anticipated from Fig. 2, 4'-hydroxy-3-aminobenzochalcone **8** (**HAB**), with a 54.0 % quantum yield, was significantly more fluorescent than its non-substituted congener **6**. This relation is validated by the further weaker quantum yield of 38.2 % of the *p*-trifluoromethyl derivative **3**. Importantly, the favourable influence of a strongly electrodonating A ring called for revision of fluorophore representation in the chalcone series, with permanent enolization of the carbonyle occurring in an extended conjugation pattern similarly to the prototypical fluorescein or rhodamine fluorophores (Fig. 3). Further, **HAB** was far more fluorescent than its 5-amino regioisomer **12** with a *ca.* 20-fold higher quantum yield.

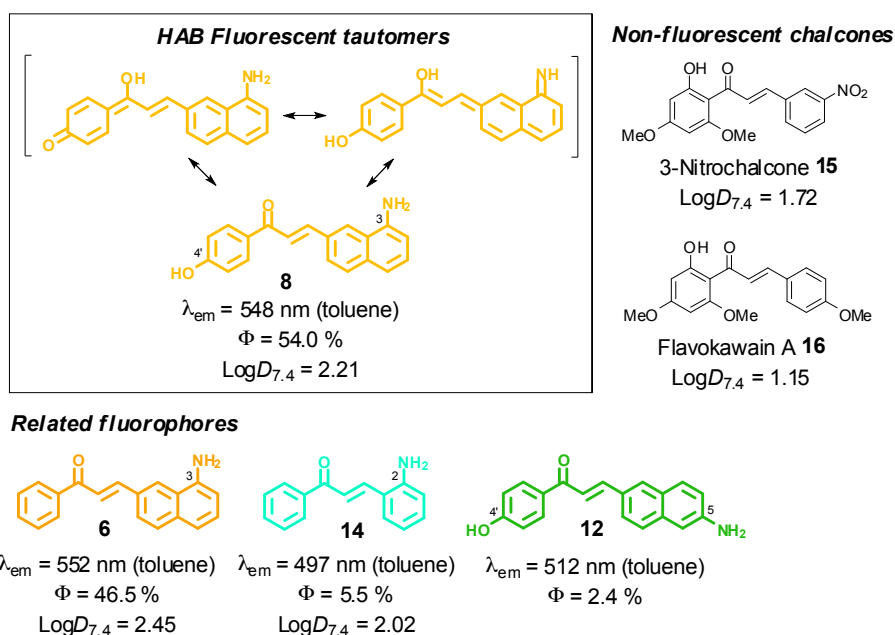


Figure 3 Structure-fluorescence relationships and $\text{log}D_{7.4}$ values at 20 °C in the 3-aminobenzochalcone, 5-aminobenzochalcone and 2-aminochalcone series (colours indicative of fluorescence emissions).

This enormous difference in quantum yield between **HAB** and **12** cannot be explained solely by conjugation patterns: **HAB** features rotational hindrance of the 3-amino group (having *peri* relationships with H-2), a phenomenon absent in the 5-amino regioisomer **12**.^{25, 26} As a result, **HAB** should be less susceptible to non-radiative desexcitation than **12**, thereby favouring fluorescence transitions. Comparing the isoelectronic compounds 3-aminobenzochalcone **6** and 2-aminochalcone **14** showed as expected that the substitution of the (B) phenyle group for a naphthyle in **6** resulted in much stronger fluorescent emission. Compound **6** thus possesses a quantum yield over eight-fold higher than **14**, the latter also displaying cyan emission and a smaller Stokes shift. Noteworthy for future biological studies, the quantum yield of 54.0 % for the most fluorescent aminobenzochalcone **HAB** is higher than those of dansylamides (*e. g.*, DPP)²⁷ and indocyanines (*e. g.*, ICG),²⁸ prototypical fluorescent probes for live-cell and live-animal imaging, respectively, and is also, to our knowledge, the highest described to date in the chalcone series (see Table S1 in the Electronic Supplementary Information).

Solvatochromic behavior. **HAB** and its non-substituted analogue **6** exhibited pronounced solvatochromism ($\Delta_{\text{max}}\lambda_{em} \sim 140$ nm), being virtually non-fluorescent in water, biological buffers and alcohols, moderately emissive in polar aprotic solvents (*e. g.*, ethyle acetate) and strongly fluorescent in non-polar solvents (*e. g.*, toluene), with the exception of alkanes. While **6** was significantly fluorescent in *n*-hexane and *n*-octane, its 4'-hydroxy derivative **HAB** proved undetectable in these solvents, and showed only weak fluorescence in *n*-alkanols used to model biological lipids (*e. g.*, *n*-heptanol) (Fig. 4a,b). Although the lack of fluorescence of **HAB** in biological buffers may be perceived as a limitation for imaging studies, it must be realized that the binding of **HAB** to amphipathic affinity sites of protein targets should result in a 4-500 fold fluorescence turn-on (FTO) according to Fig. 4b.¹⁰ As a proof-of-principle, bovine serum albumin (BSA) quenched **HAB** weak blue fluorescence ($\lambda_{ex} = 360 \text{ nm}$, $\lambda_{em} = 445 \text{ nm}$) in a dose-response manner while inducing the formation of a strongly yellow-emitting **HAB**-protein fluorescent complex ($\lambda_{ex} = 420 \text{ nm}$, $\lambda_{em} = 578 \text{ nm}$) (Fig. 4e-f). A FTO of 21.5 (excitation at 420 nm, at BSA concentration of 10 mg/ml) was observed upon binding of **HAB** to the protein (Fig. 4f), associated to an important bathochromic shift of its fluorescence spectrum ($\Delta\lambda_{ex} = 60 \text{ nm}$, $\Delta\lambda_{em} = 133 \text{ nm}$) which was similar to that obtained in the polar aprotic solvent DMF (Fig. 4d,f). This behaviour is opposite to that of chalcones binding the physiological sites of BSA and displaying slight ipsochromic shifts and quenching effects indicative of an apolar environment,¹⁸ suggesting that **HAB** binds non-conventional BSA sites. Overall, **HAB** should be featured with high signal-to-noise ratio and elevated pharmacological sensitivity, low or negligible predicted fluorescence in compartments such as the extracellular medium, the cytosol and the membranes under free form, and high fluorescence when target-bound ("in-target" fluorogenesis). Moreover, its absence of fluorescence in water or buffers has the potential to greatly simplify and time-optimize the staining protocols, with suppression of tedious washing steps and diffusion liabilities following dye administration.

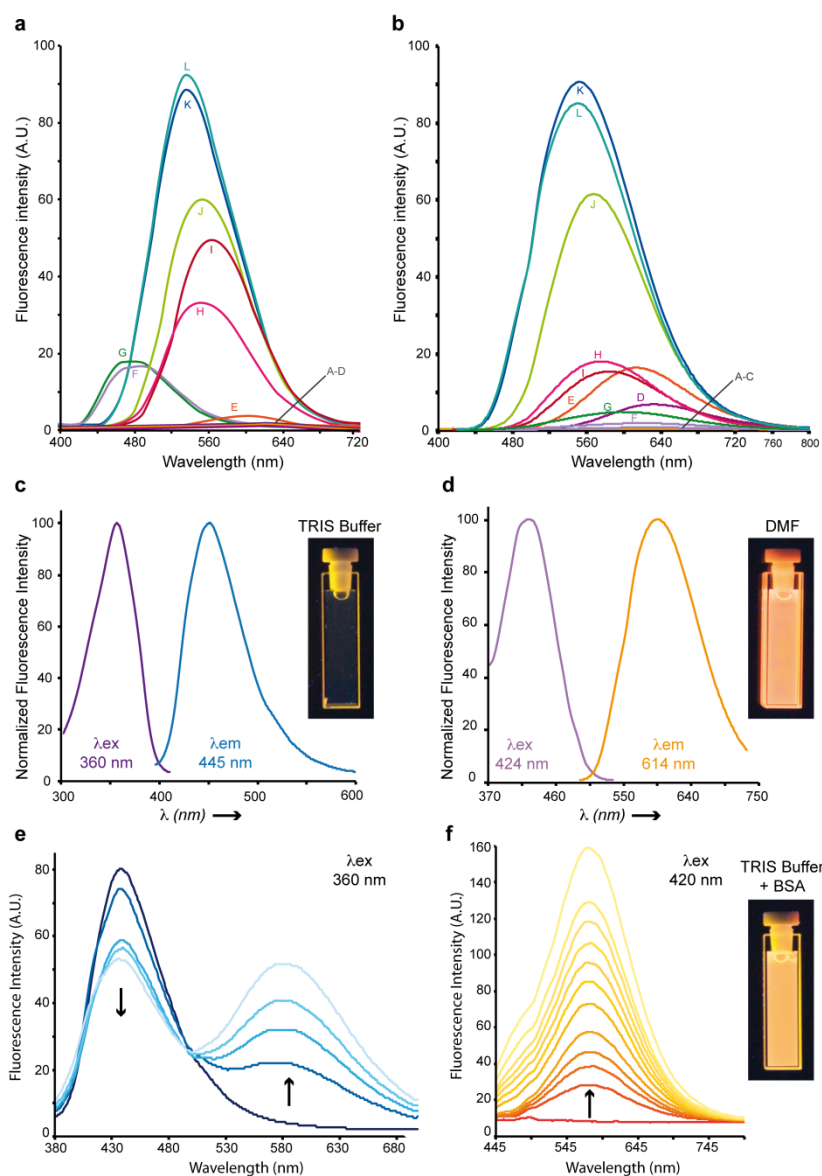


Figure 4 HAB shows strong solvatochromism and protein-dependent fluorogenesis. (a,b) Semi-quantitative emission spectra of 3-aminobenzochalcone **6** (Fig. 4a) and HAB (Fig. 4b) in various solvents (50 μ M). A : H₂O ; B : TRIS buffer 10 mM, pH 7, NaCl 100 mM, MgCl₂ 5 mM ; C : AcOH ; D : DMSO ; E : MeCN ; H : CHCl₃ ; I : AcOEt ; J : 1,4-dioxane ; K : benzene ; L : toluene. Dissimilar solvent lettering between the figures are F : *n*-hexane ; G : *n*-octane (Fig. 3a) and F : *n*-butanol ; G : *n*-heptanol (Fig. 3b). (c,d) Normalized excitation spectra (purple lines) and fluorescence emission spectra (blue or orange lines) of HAB (50 μ M) in TRIS buffer pH 7.0 (TRIS.HCl 10 mM, NaCl 100 mM, MgCl₂ 5 mM) (c) or DMF (d). (e) Fluorescence emission spectra of HAB (50 μ M) titrated by BSA (0 to 1 mg/mL) in TRIS buffer with an excitation wavelength of 360 nm. (f) Fluorescence emission spectra of HAB (50 μ M) titrated by BSA (1 to 10 mg/mL) in TRIS buffer with an excitation wavelength of 420 nm. Arrows indicate the decrease or increase in fluorescence following the addition of BSA. UVA-irradiated cuvettes in the corresponding conditions are shown as insets in (c), (d) and (f).

Cytopermeability evaluation. Lipophilicity is a key physicochemical parameter affecting cellular penetration and subcellular distribution *in vitro*, as well as pharmacokinetics *in vivo*.²⁹ We measured the partition coefficients of key benzochalcones compared to reference chalcones using *n*-octanol and pH 7.4 phosphate buffered saline (PBS), as to draw structure-cytopermeability relationships in this novel series (Fig. 3). As expected, the favorable influence of a naphthyle *vs* a phenyl ring regarding fluorescence was also exerted in terms of lipophilicity, as 3-aminobenzochalcone **6** and HAB possessed log $D_{7.4}$ values significantly higher than that of mere 2-aminochalcone **14**. In particular, **6** was almost three times more lipophilic than its exact 2-aminochalcone congener **14**. On the other hand, the presence of a 4'-hydroxy group on HAB made it 2-fold more hydrophilic than its 4'-deshydroxy congener **6**. Further, HAB was three to eleven times more lipophilic than 3-nitrochalcone **15** and natural flavokawain A **16** chosen as representative biologically-active chalcones^{30, 31} (Fig. 3). Overall, the neat amphipathicity (log $D_{7.4}$ between 1.5 and 2.5), neutrality as well as small molecular weight (289.3 Da) of HAB³² predict an optimal histopermeability for this compound, which thus could behave as a fast-acting fluorescent probe *in vivo*.

HAB labels specific cells in live zebrafish embryos and swimming larvae. HAB, the most fluorescent, solvatochromic and histopermeable derivative obtained, was tested in representative transparent animal models. We chose the nematode *Caenorhabditis elegans* and the zebrafish *Danio rerio* to study the cell and organelle distribution of HAB in complete live systems and assess its biological specificity. HAB could not be microscopically visualized in *C. elegans* due to excessive autofluorescence of the nematode (data not shown). On the other hand, HAB displayed a unique labeling pattern in zebrafish that deserved in-depth investigation. When HAB was incubated at 10 μM for 60 min on live zebrafish embryos and swimming larvae ranging from 24 hours post-fertilization (hpf) to 72 hpf, fluorescence emission was detected mainly in the 550-650 nm window following excitation at 488 nm, indicative of a non-aqueous environment (see Fig. 4b for the solvatochromic properties of HAB, and Fig. S2 in the Electronic Supplementary Information for the emission spectrum of HAB *in vivo*). Since the fluo-labeling was maximal in the yellow-orange region of the visible spectrum, this suggested that HAB bound to specific proteins with strong target-induced bathochromic fluorogenesis and FTOs (Fig. 4e-h). This labeling displayed a neat pattern of punctuated areas that first appeared by 32 hpf in the ventral tail of the embryo (Fig. 5a,e). The number and intensity of HAB fluorescent spots progressively increased at 48 hpf and 72 hpf following the known deployment of macrophages and neutrophils during zebrafish development,^{4, 5} suggesting that these cell types could be targeted by HAB. The shape and size of the fluorescent spots within the caudal region of the specimens suggested labeling of some subcellular compartment rather than whole cells.⁵ Noteworthy, the already autofluorescent pigment cells present in 72 hpf larva underwent a significant increase of fluorescence in presence of HAB (Fig. 4c,d) suggesting that the probe also accumulated within these cells due to their high content in aromatic pigments (i. e., pteridine and guanine derivatives).^{33, 34}

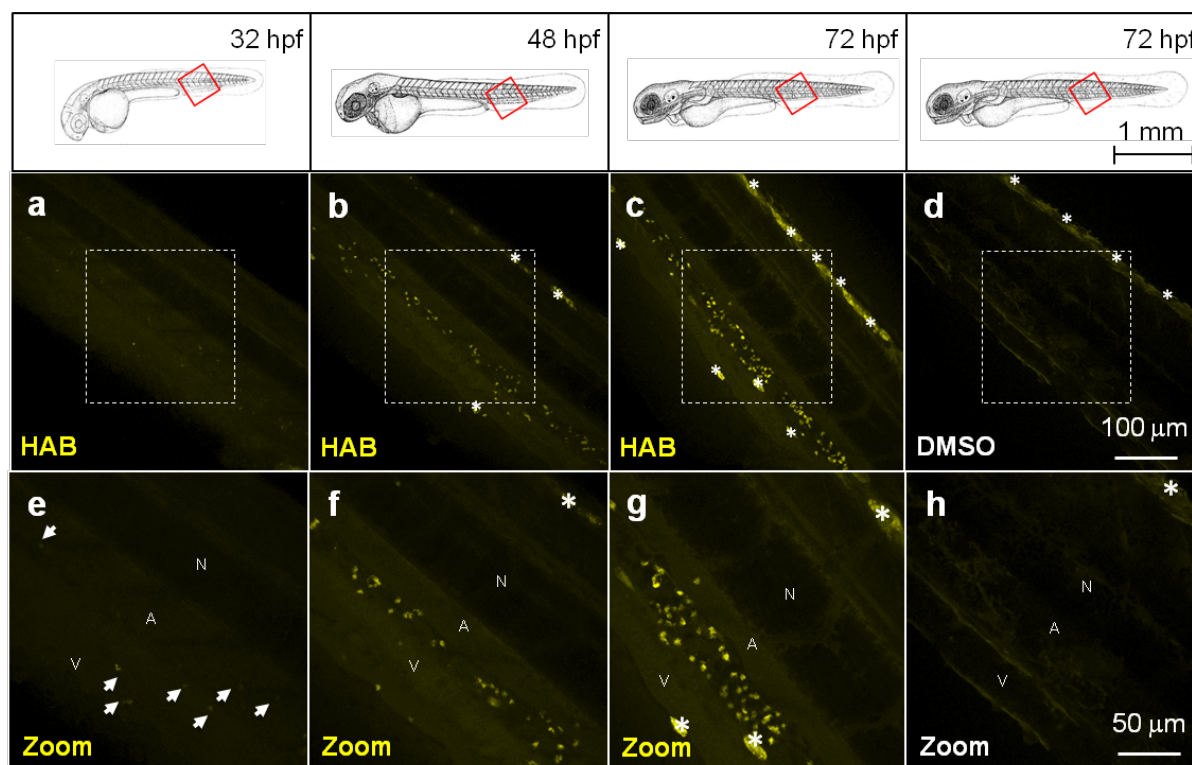


Figure 5 HAB labels specific cells in live zebrafish from 32 hpf. Confocal fluorescence imaging of HAB labeling (10 μM) in live wild-type zebrafish embryos (32 and 48 hpf) and swimming larvae (72 hpf) following excitation at 488 nm and detection in the 550-650 nm range. The yellow-orange color is indicative of the fluorescence seen with the naked eye. Maximum intensity Z-projection images (2 μm serial optical sections) are shown. Arrows point to HAB label; asterisks mark pigment cells. A, artery; N, notochord; V, vein.

HAB labeling is reversible. HAB labeling was found to be fairly photostable in the conditions used so far, with *ca.* 50 % fluorescence lost after 30 min of continuous illumination at 488 nm. However, since the embryos and larvae were systematically washed and mounted in HAB-free agarose for live imaging, the diffusion of HAB outside of its binding sites might be responsible for the loss of labeling overtime. To discriminate between free diffusion and photobleaching as the two possible causes for signal loss, we performed time-lapse imaging experiments in which either of these two phenomena was kept to a minimum. To test the free diffusion hypothesis, 72 hpf zebrafish larvae were treated with 10 μM HAB for 1 hr, washed and mounted in tracer-free mounting medium, then imaged over time with short exposure-acquisition pulses every 10 min. Under these conditions of lower illumination hence limited photobleaching, the detection of HAB-labeled structures was no longer possible after *ca.* 1 hr, with again *ca.* 50 % of fluorescence lost after 30 min exposure (see Figure S3 in the Electronic Supplementary Information). To test the photobleaching hypothesis, we treated the 72 hpf larvae with

10 μM **HAB** for 1 hr and mounted them in agarose and tricaine containing 10 μM **HAB**. We then imaged the zebrafish larva embedded in **HAB** 10 μM over time under continuous illumination (indicate time lapse here) by the 488 nm laser. Under these conditions of maximum photobleaching and abolished free diffusion, **HAB** labeling proved highly photostable, as it could be detected for up to 15 hrs of time-lapse imaging (see Video S4 in the Electronic Supplementary Information). This observation indicates that **HAB** bound *in vivo* continually exchanges with free non-fluorescent **HAB**, at a rate faster than the photobleaching of the bound **HAB** during continuous 488 nm laser illumination. This remarkable feature makes **HAB** an ideal live stain for both long-term and high temporal resolution confocal imaging of neutrophil granules in the zebrafish. These conditions of constant equilibrium by continuous contact, made possible by the absence of **HAB** fluorescence in aqueous media, constitute optimal settings for **HAB** labeling on the zebrafish model and are particularly suitable for long-term experiments.

HAB labels neutrophil granules in live zebrafish larvae. To identify the cell type(s) labeled by **HAB**, that according to their localization and developmental timing of detection could be the first leukocytes of the zebrafish embryo and larva (macrophages and/or neutrophils), we stained zebrafish transgenic 72 hpf larvae harbouring fluorescent macrophages or neutrophils³⁵⁻³⁷ with **HAB**. Upon treatment with 10 μM **HAB** of Tg(Mfap4:mCherry-F) larvae possessing red-fluorescent macrophages expressing mCherry, we found that the probe did not co-localize with the red-fluorescent macrophages (Fig. 6a-d). Due to the wide emission range of the mCherry protein (560-760 nm), that overlapped with that of the yellow-green emitting **HAB**, mCherry was imaged following excitation at 552 nm and collecting only the “far red” portion of its fluorescence emission (660-750 nm), and **HAB** was excited at 448 nm and collecting the 550 - 650 nm range of its emission spectrum. Upon treatment with 10 μM **HAB** of Tg(mpx:GAL4/UAS-E1b:nsfB-mCherry) larvae with neutrophils expressing mCherry in their cytoplasm and using the same **HAB**/mCherry acquisition parameters as above, we could show that **HAB** perfectly colocalized with all neutrophils of the imaged ventral tail region, labeling a specific compartment within them. (Fig. 6e-h). Using GFP-labeled neutrophils (Tg(mpx:GFP) strain), and sequentially detecting GFP emission in the 500-520 nm range and **HAB** using the “red” portion of its emission spectrum (> 600 nm) by exciting both fluorophores by the 448nm laser (Fig. 6i-l) we confirmed that **HAB** targeted a neutrophil specific compartment. Not only did **HAB** stained all neutrophils of the ventral tail region of 72 hpf larvae, where they are known to be particularly abundant^{2, 4, 37}, but **HAB**-labeled neutrophils could also found in the eye, ear and yolk of 72 hpf larvae (data not shown), indicating that **HAB** labels the entire neutrophil population *in vivo*. Collectively, these observations demonstrated that zebrafish neutrophils are the cell type selectively targeted by **HAB**, where it specifically labels a compartment within these cells. To identify the compartment targeted by **HAB** within neutrophils, we performed high-resolution confocal imaging of **HAB**-labeled cells in 72 hpf larvae harbouring red neutrophils combining the fluorescence detection of **HAB** and mCherry with DIC microscopy. **HAB** was found to co-localize with neutrophil granules, which are easily recognizable in transmitted light / DIC imaging^{5, 38} for they are refractile and constantly moving in the cytoplasm (Fig. 6m-p). This colocalization was unambiguously demonstrated by the perfect overlap of fluorescence **HAB** signals and DIC images during time-lapse acquisitions of live patrolling neutrophils (see high-resolution Videos S5 and S6 in the Electronic Supplementary Information). Similar to their mammalian counterpart, the granules of zebrafish neutrophils contain myeloperoxidase.^{2, 38, 39} The diazo dye Sudan Black B (SB) is a classical lipid stain that specifically labels the myeloperoxidase-positive granules of zebrafish neutrophils,^{5, 40} as also observed in human neutrophils.^{41, 42} The first SB-stained granules are detected by 33-35 hpf in zebrafish embryos, within the first, still immature embryonic neutrophils; this staining then increases in number and intensity, revealing the deployment of neutrophils during zebrafish development.⁵ To check that **HAB** was targeting the same granule population as SB in neutrophils, we tried to combine the two dyes. We first tested if the **HAB** label was compatible with the fixation protocol classically used to fix zebrafish embryos and larvae, but failed to detect **HAB** labeling in the larva post-fixation for two hours at room temperature with either 1 or 4 % formaldehyde, or when performing **HAB** labeling before the fixation. This could be due to the loss of **HAB** pharmacology in fixed samples, or to the reaction of **HAB** with formaldehyde, leading to fluorophore destruction: eventhough **HAB** is both a very weak organic base (predicted pK_a value of 3.97 for its amino tautomers, see Figure S7 in the Electronic Supplementary Information) and a weak nucleophile, possessing the electronic features of a vinylogous amide, this possibility cannot be ruled out in absence of dedicated study. In any case, it was not possible to combine the SB staining with the **HAB** labeling.

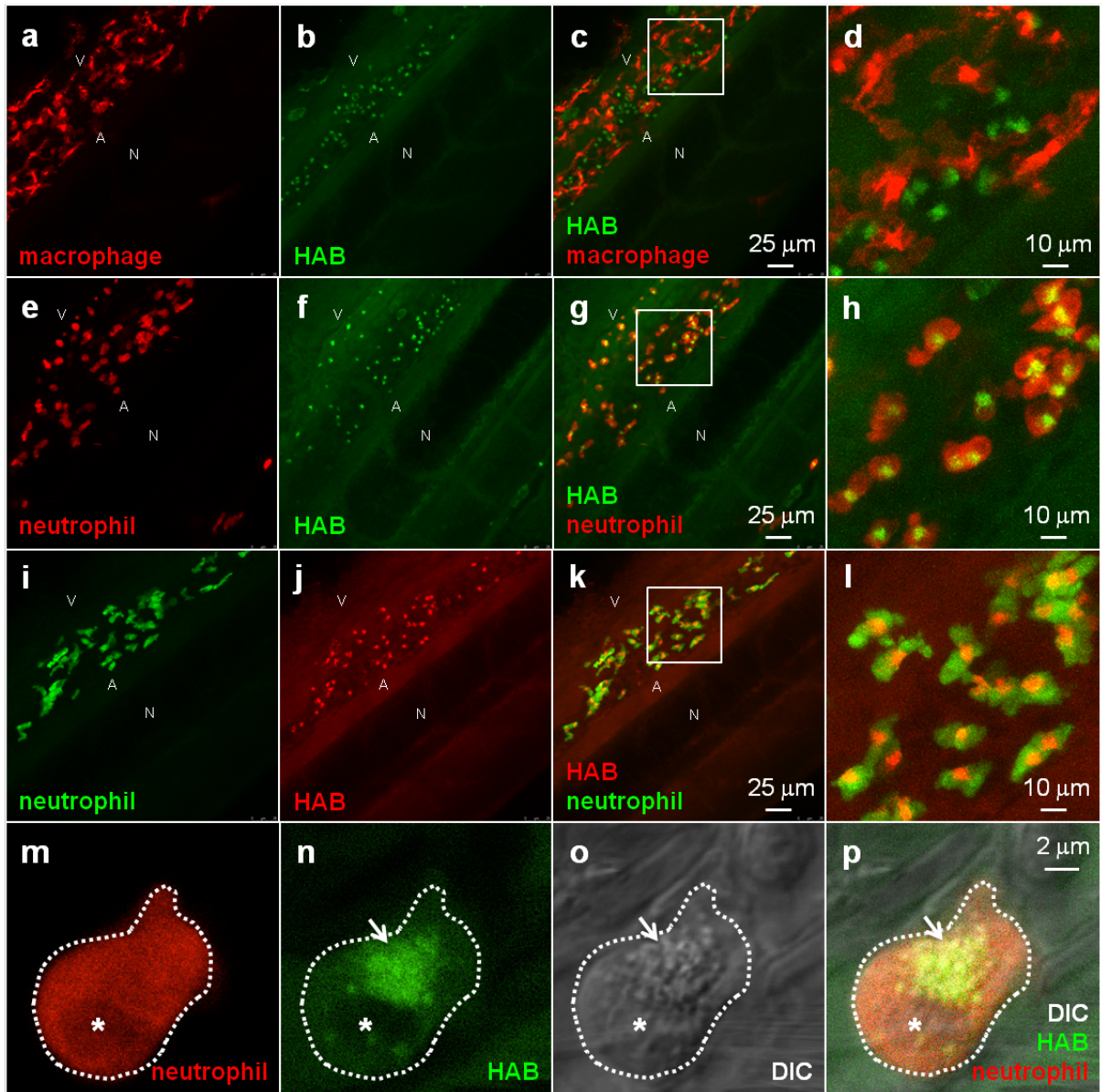


Figure 6 HAB labels zebrafish neutrophil granules. (a-l) Confocal fluorescence imaging of **HAB** (10 μ M) in live transgenic 72 hpf zebrafish larvae following excitation at 448 nm under equilibrium conditions. Detection parameters were as follow: for **HAB** / mCherry: λ_{EX} 448 nm, λ_{EM} 550-650 nm, mCherry: λ_{EX} 552 nm, λ_{EM} 660-750 nm using sequential modes of acquisition. For GFP / **HAB**: GFP λ_{EX} 448 nm, λ_{EM} 500-520 nm, **HAB**: λ_{EX} 448 nm, λ_{EM} 550-650 nm using sequential modes of acquisition. Maximum intensity Z-projection images (2 μ m serial optical sections) are shown. (m-p) High-resolution DIC and confocal fluorescence imaging of **HAB** (10 μ M) in live 72 hpf zebrafish larva harbouring red neutrophils. Arrows point to **HAB**-labeled granules according to the DIC images in neutrophils. A single 0.4 μ m optical section is shown. Boxes in Fig. 6c,g,k indicate the regions magnified in the insets (Fig. 6d,h,l respectively). Abbreviations used: A (aorta); N (notochord); V (vein); asterisk = nucleus. See Electronic Supplementary Information for Videos S5 and S6 related to Fig. 6m-p.

HAB reveals the behavior of neutrophil granules during phagocytosis in live zebrafish larva. To circumvent this technical limitation, we sought indirect evidence for the identity of neutrophil granules as the targets of **HAB**. One of the most important functions of neutrophils is to eliminate invading microorganisms. Neutrophils are highly phagocytic cells, able to engulf and kill microbes with the arsenal of microbicidal compounds stored in their granules. Once they have engulfed microbes, neutrophils release the granule content (e.g., myeloperoxidase-produced hypochlorous acid and proteases) into the phagosome. We have shown that *in vivo*, zebrafish neutrophils degranulate into the phagosome following microbe phagocytosis and that the myeloperoxidase activity initially contained in the granules often relocates to the phagosome, while the SB staining correlatively disappears.⁴³ These steps have been advantageously reproduced with opsonized zymosan particles in cultured mammalian neutrophils, to show that neutrophil granules are recruited to the nascent phagosome in which they deliver their content by exocytosis.^{8,44} To determine whether **HAB** would allow the visualization of neutrophil granule dynamics during phagocytosis *in vivo*, we vitally stained a zebrafish larva with **HAB**, then

subcutaneously injected red-fluorescent Cy5-zymosan, and immediately monitored the interaction between **HAB**-labeled neutrophil granules and zymosan particles by high resolution confocal imaging (Fig. 7). We found that upon zymosan phagocytosis, **HAB**-labeled granules are massively recruited to the particle-containing phagosomes (Fig. 7a,b,d and related Video S8 in ESI), similar to the myeloperoxidase containing, SB-labeled granules which relocalised around the zymosan-containing phagosome in the fixed larva (Fig. 7c). These observations strongly suggest that the myeloperoxidase-containing granules are the targets of **HAB** *in vivo*. They also represent, to our knowledge, the first documentation of the dynamics of neutrophil degranulation upon phagocytosis in an entire live organism.

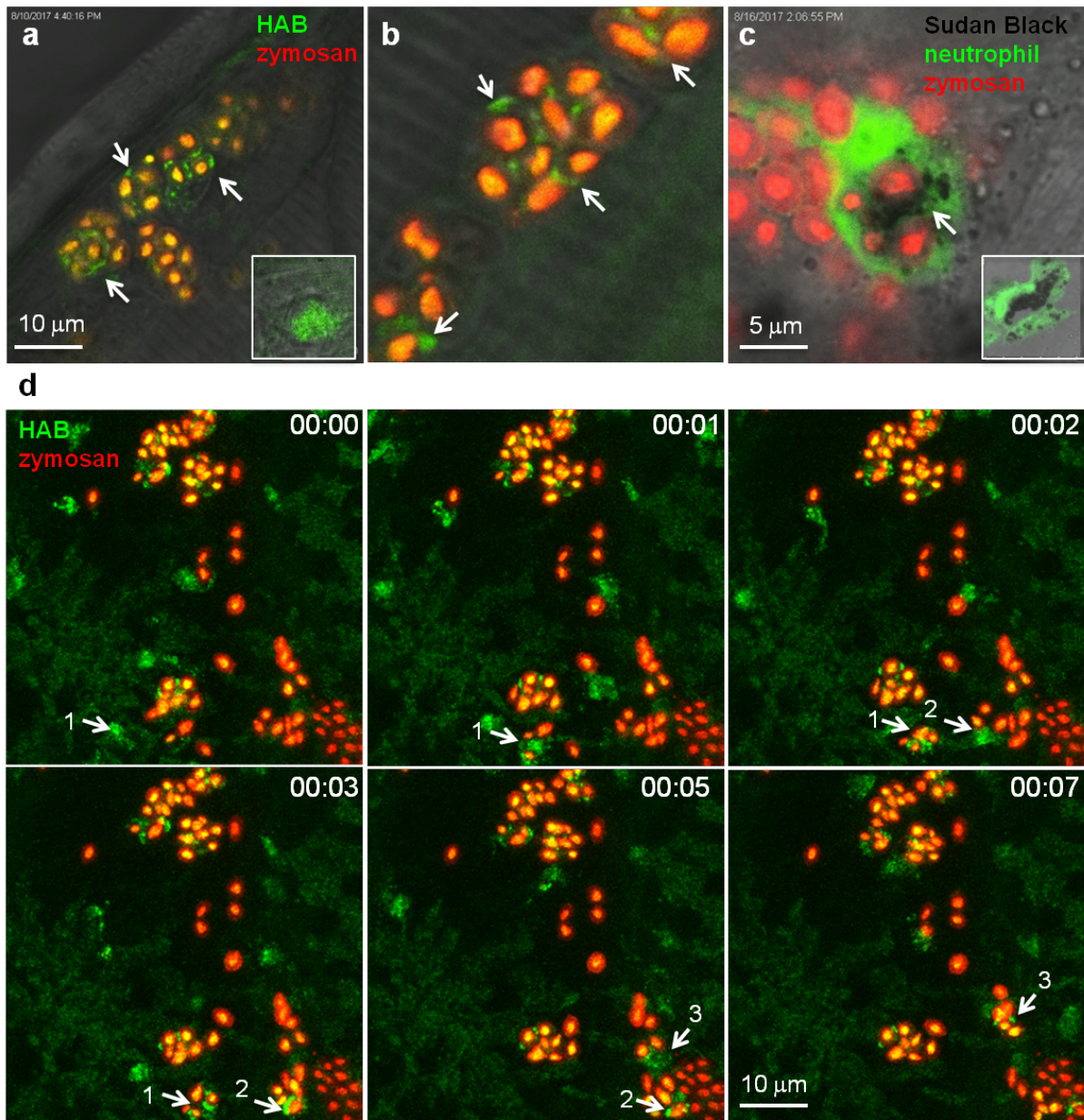


Figure 7 HAB reveals the dynamics of neutrophil granules upon phagocytosis of zymosan particles in live zebrafish. (a,b) Confocal live imaging of **HAB**-labeled neutrophil granules upon phagocytosis of subcutaneously-injected zymosan in a live 72 hpf zebrafish larva under equilibrium conditions. **HAB** is recruited to the forming phagosomes (arrows). Inset: **HAB** labeling of resting neutrophil. (c) Sudan Black (SB) staining of myeloperoxidase-containing neutrophil granules showing granule recruitment to the phagosome upon zymosan phagocytosis in fixed zebrafish larva. Inset: SB staining of a resting neutrophil; A single 1 μ m optical section is shown. (d) Frames extracted from an *in vivo* time-lapse confocal imaging sequence (time step = 1 min). Arrows point to **HAB**-labeled neutrophil granules that are recruited to the nascent zymosan containing phagosome. Three neutrophils (pointed with number 1 to 3) were tracked during the time lapse sequence. Maximum intensity Z-projection (1 μ m serial optical sections). See Electronic Supplementary Information for Video S8 related to Fig. 7d.

HAB does not target neutrophil myeloperoxidase, and the staining of neutrophil granules by HAB is not a general feature of chalcones. To tentatively identify the specific protein target of **HAB** in the neutrophil granules, we performed **HAB** labeling in myeloperoxidase knock-out zebrafish larvae (“spotless” strain) under equilibrium conditions.⁴⁵ While mutant larvae showed the expected absence of SB staining, they nevertheless still exhibited a fluorescent labeling with **HAB** qualitatively and quantitatively indistinguishable from wild-type larvae (Fig. 8a-c). This result shows that the myeloperoxidase abundant in neutrophil granules is not the biochemical target of **HAB**. We also tested a selection of biologically-active chalcones as possible **HAB** competitors, based on their known or putative action on neutrophils such as inhibition of myeloperoxidase activity or repressing effects on pro-inflammatory mediators such as NF- κ B, TNF- α , COX-2 and various interleukines.⁴⁶⁻⁴⁸ The natural chalcones flavokawain A **16** and cardamonin **17** are potent anti-inflammatory, proapoptotic and antitumour agents in mouse models, due to their ability to block NF- κ B signaling.^{31, 49-51} Synthetic chalcone **18** is an inhibitor of chemokine CXCL12 that blocks its binding to several chemokine receptors, preventing eosinophil infiltration in an asthma mouse model.⁵² 3-nitrochalcone **15** possesses pronounced antinociceptive properties in mice that are anti-inflammatory in origin.⁵³ Last, 4-methylchalcone **19** was selected due to its homology with mere (unsubstituted) chalcone, reported to exert anti-myeloperoxidase and anti-migratory effects on zebrafish neutrophils.⁴⁶ Larvae were first incubated with the competitors alone at 100 μ M for 1 hr to assess their toxicity, as well as possible basal fluorescence in the zebrafish. Under these conditions, all specimens remain alive with no apparent toxicity from the chalcones. Moreover, using the same detection settings than for **HAB** at 10 μ M (λ_{EX} 488 nm, λ_{EM} 550-650 nm), none of the competitors showed fluorescence and their labeling was undistinguishable from that of the negative control DMSO (data not shown), except for chalcone **18** (see below and Fig. S9 in the Electronic Supplementary Information). When these various potential competitors were co-incubated at 100 μ M with **HAB** at 10 μ M in the same conditions, we could observe no extinction or diminution of **HAB** fluorescence *in vivo* with any of these competitors relative to the control (Fig. 8e-j). Moreover, fluorimetric association experiments in TRIS buffer or DMF (where **HAB** shows the same type of yellow-orange fluorescence as in neutrophil granules, see Fig. 4d) demonstrated that none of these chalcones, when incubated in presence of **HAB** at the same 10:1 stoichiometry, induced any significant qualitative or quantitative change in **HAB** fluorescence. The only exception was chalcone **18** which caused strong emission quenching in both media (data not shown), a feature not at play in zebrafish larvae *in vivo* (Fig. 8g). The binding of **HAB** to neutrophil granules thus appears to be the result of the probe’s precise physicochemical signature, rather than a general feature of chalcones.

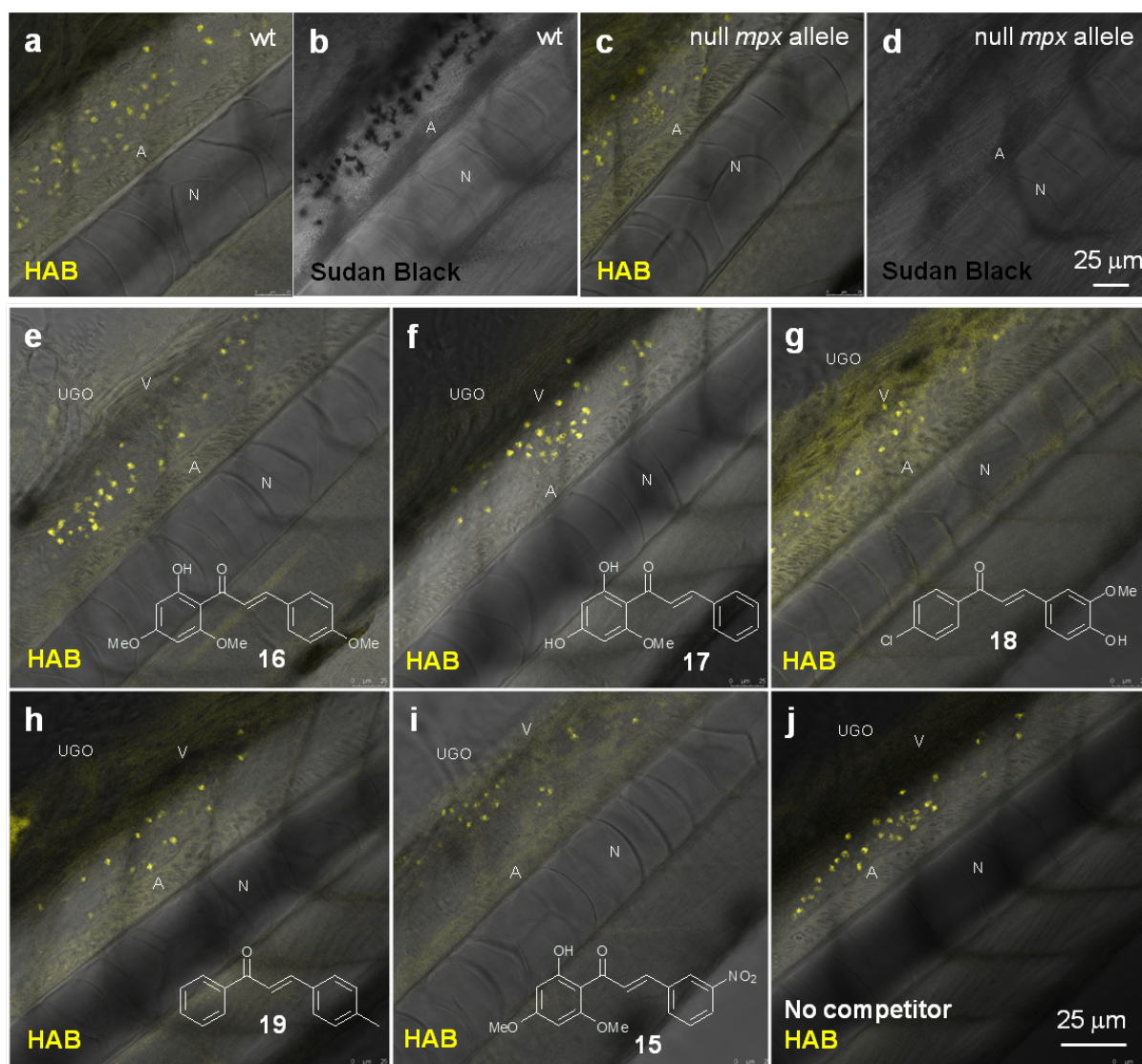


Figure 8 HAB does not target zebrafish neutrophil myeloperoxidase, and its binding to neutrophil granules is not a general feature of chalcones. (a,c) Merged confocal fluorescence and bright-field imaging of HAB (10 μ M) in live wild-type (a) or “Spotless” (NL 144_01 mutant: null *mpx* allele) (c) 72 hpf zebrafish larvae following excitation at 488 nm and detection in the 550-650 nm range under equilibrium conditions. (b,d) SB staining of myeloperoxidase-containing neutrophil granules in bright-field imaging. (e-j) Merged confocal fluorescence and bright-field imaging of HAB (10 μ M) in live wild-type 72 hpf zebrafish larvae co-treated with chalcones **15**, **16** (flavokawain A), **17** (cardamomin), **18** or **19** (100 μ M) following excitation at 488 nm and detection in the 550-650 nm range under diffusion conditions. The yellow-orange color is indicative of the fluorescence seen with the naked eye. Single 2 μ m optical sections are shown. Abbreviations used: A (aorta); N (notochord); UGO (urogenital opening); V (vein).

During the course of this competition study, we discovered that 4-hydroxy-3-methoxy-4'-chlorochalcone (Cpd. **18**) at 100 μ M was responsible for unusual fluorescence in presence of HAB (Fig. 8g), and deserved further investigation. When incubated alone at the same concentration on 72 hpf larvae and excited at 488 nm, chalcone **18** exhibited a green-yellow fluorescence that illuminated the anatomy of the specimens. Indeed, confocal imaging showed that the fluorescence of **18** delineated the trunk neuromasts, somite muscle fibers and boundaries, blood vessels, notochord, spinal cord, spinal canal and caudal hematopoietic tissue (Fig. S9 in the Electronic Supplementary Information). Detailed examination revealed no detectable intracellular staining, but interstitial histological labeling. This behavior is reminiscent of that of BODIPY-ceramide, a fluorescent dye previously used at similarly high concentration as a histological counterstain for the confocal imaging of live zebrafish embryos.^{54, 55} The fact that chalcone **18** was not cytopermeable even at high concentration further validates the global design of HAB, a benzochalcone congener, as a histo- and cytopermeable tracer for *in vivo* studies. Interestingly, chalcone **18** was recently evaluated in the zebrafish model as an inhibitor of the chemokine CXCL12a, for its activity against the collective migration of cells of the posterior lateral line primordium. At 10 μ M, **18** showed moderate biological effects and was not fluorescently detected by GFP filters.⁵⁶ The complete study of chalcone **18** regarding

fluorescence detection threshold, photostability, phenotypic effects and long-term toxicity is currently underway, in order to validate this compound as a novel anatomical interstitial live stain in the zebrafish model.

HAB labels granules in live human primary neutrophils. In order to validate **HAB** as a specific vital stain of neutrophil granules not only in fish but also in mammals, and to assess its relevance for human studies, we attempted the **HAB** labeling of live primary human neutrophils freshly isolated from total blood. Human neutrophils exist under two morphologically- and phenotypically-distinct types depending on their state of activation. Whereas non-activated neutrophils consist in round-shaped non-adhering circulating cells, activated neutrophils are polyhedral cells expressing a number of cytoadhesins and adhering to endothelium walls, glass or plastic surfaces.^{57, 58} When stained with 10 μ M **HAB**, non-activated neutrophils exhibited intense but diffuse fluorescent labeling, presumably due to the difficulty of resolving subcellular structures when imaging non-adherent cells (Fig. 9a-c). An equally intense labeling of cells at the level of subcellular granular structures was detected in the same conditions in activated neutrophils, consistent with the morphology and distribution of human neutrophil granules,^{59, 60} in addition to a strong perinuclear staining possibly corresponding to the nuclear membrane (Fig. 9d-f and S10 in the Electronic Supplementary Information). To address the human blood cell selectivity issue, we assessed **HAB** labeling on other freshly-isolated cell populations from whole human blood (peripheral blood mononuclear cells, PBMC) in the same conditions than those used to image purified neutrophils. **HAB** was found to exhibit an impressive selectivity for neutrophils over lymphocytes, monocytes, erythrocytes and thrombocytes (platelets), that were all weakly to faintly labeled (Fig 9g-i). This selectivity seems to be the result of the accumulation of **HAB** in neutrophil granules, consistent with the complete cell and organelle specificity observed in the zebrafish model *in vivo*. Although these results deserve further investigation regarding the subset of granules labeled in human neutrophils,⁵⁹ they constitute a strong presumption that the specific labeling of neutrophil granules by **HAB** in the zebrafish model is also relevant in mammalian systems.

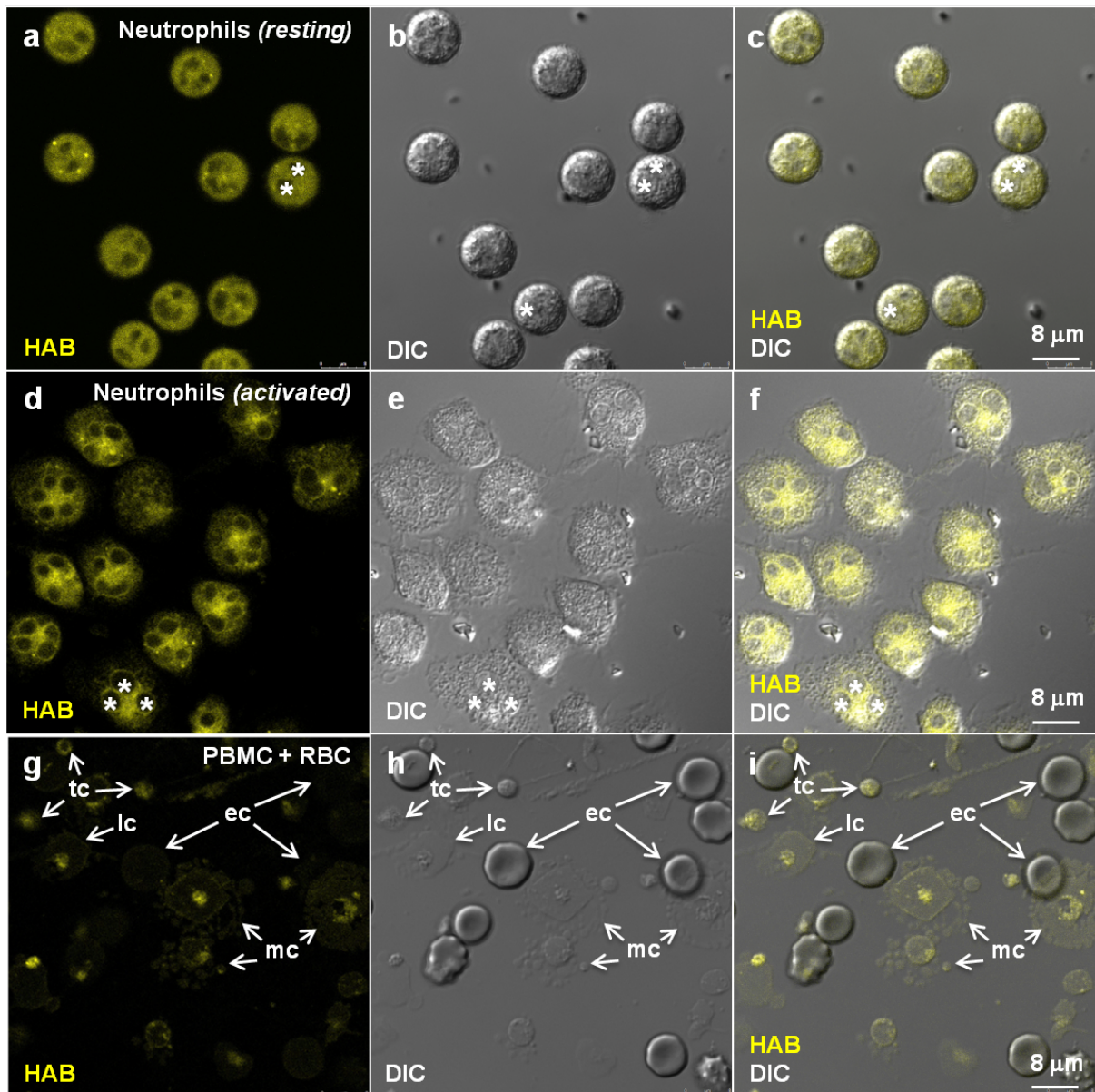


Figure 9 HAB selectively labels live human primary neutrophils over other blood cell types. (a-c) and (d-f): Confocal fluorescence and DIC imaging of HAB (10 μ M) in live human neutrophils following excitation at 448 nm and detection in the 550-650 nm range. Single 0.4 μ m optical sections are shown. (a-c) show resting, non-activated, non-adherent neutrophils. (d-f) show activated, adherent neutrophils: note HAB staining of neutrophils granules; (g-i): Confocal fluorescence and DIC imaging of HAB (10 μ M) in live human lymphocytes (lc), erythrocytes (ec), monocytes (mc) and thrombocytes (tc) using the same settings than in (a-c) and (d-f). Single 0.4 μ m optical sections are shown. The yellow-orange color is indicative of the fluorescence seen with the naked eye. Asterisk = nucleus.

Discussion

A novel 3-aminobenzochalcone, **HAB**, was rationally designed, synthesized and validated as a histopermeable and fluorogenic vital stain for *in vivo* biological studies. Photophysically, **HAB** has elevated Stokes shift, the highest fluorescence quantum yield described to date in this series, elevated signal-to-noise ratio upon protein binding, and unprecedented photostability. This also chemically very stable tracer possesses the minimal architecture to be strongly fluorescent, and stains neutrophils in zebrafish embryo and larva with extraordinary specificity, with no labeling of other, even related, cell types (e. g., macrophages). Subcellularly, **HAB** proved specific of zebrafish neutrophil granules, with no staining of other organelles or compartments. This behavior was rationalized as target-induced bathochromic fluorogenesis based on various chemical and biochemical model systems. Neutrophil labeling was independent of the state of cell activation, since **HAB** stained the granules of both resting and phagocytically-active neutrophils with equal intensity and specificity. **HAB** labeling in the zebrafish followed the deployment of neutrophil from 32 hpf embryo to 72 hpf swimming larva and was even visualised in neutrophil granules in 6 day-old larva with similar sensitivity despite the increase in tissue density and thickness (see Fig. S11 in the Electronic Supplementary Information). Due to its absence of toxicity up to 48 hrs incubation

and outstanding photostability, **HAB** is ideal for the long-term, high temporal resolution live imaging of developing zebrafish, with the potential of dynamic monitoring of the neutrophil granules in virtually any physiological or physiopathological context. To our knowledge, no other related tracer is endowed with such precious characteristics. Last, **HAB** intensely labeled freshly purified neutrophils from human blood at the level of granular structures consistent with neutrophil granules. Fluorescent dyes for neutrophil granules are limited, including quinacrine (QA),⁸ LysoTrackerRed[®] (LTR),⁹ dihydrorhodamine (DHR) 123,⁹ and rhodamine-thiolactones (RTLs),⁶¹ which are non-specific by essence. QA and LTR as weak bases constitute general acidotropic stains, sequestered under their protonated form in various low pH organelles and vesicles (e. g., lysosomes,⁶²⁻⁶⁴ apoptotic vesicles,⁶⁵ mast cell granules^{66, 67}), to which mammalian basophil and neutrophil secreted granules also belong.^{68, 69} DHR 123 and RTLs are part of ROS-activated profluorophores used to detect hydrogen peroxide/peroxynitrite and hypochlorous acid, respectively, in activated neutrophils as well as in various other cell systems and organelles.^{61, 70-72} A comparative analysis of the various existing tracers of neutrophil granules is provided in Table 1. In marked contrast, the unique staining of live zebrafish neutrophil granules by **HAB** over other cell types and acidic compartments in the whole organism, together with **HAB** very weak basicity (about 10⁵-fold lower than that of acidotropic amines⁶³ with predicted pK_a value of 3.97 for the amino tautomers, see Figure S7 in the Electronic Supplementary Information), supports a specific target-induced labeling of neutrophil granules by **HAB**. Although we showed that the myeloperoxidase present in the granules as is not involved in their specific staining by **HAB**, these granules also contain abundant neutral serine proteases (e. g., elastase, proteinase 3, cathepsin G),⁵⁹ which constitute putative biochemical targets for **HAB** based on their reactivity towards reversible electrophilic inhibitors.^{73, 74} In this context, **HAB** has an immediate surrogate for proteomic interrogation under the form of a photoalkylative azido analogue (Fig. 1) easily accessible through Sandmeyer-type modification of the aromatic amino group.²² The covalent photolabeling of live zebrafish larvae or isolated human neutrophils with a fluorogenic 3-azido-4'-hydroxybenzochalcone, FACS purification of labeled cells followed by Western Blot identification of the covalently-stained molecular target(s) of **HAB**, therefore seems within reach. Overall, due to its optimal photophysical and physicochemical properties and unprecedented biological specificity, **HAB** constitutes a valuable small-molecule addition to the fluorescent proteins toolbox used in the zebrafish model, which it functionally and spectrally complements, and appears suitable for functional studies in live mammalian neutrophils. **HAB** therefore holds great promise as a vital stain to monitor the dynamics and behaviour of neutrophil granules in various aspects of the neutrophil function in the context of a live organism, with potential relevance to human physiology and physiopathology.

Table 1 Functional comparison of HAB with existing tracers of neutrophil granules

TRACER	SPECIFICITY FOR NEUTROPHIL GRANULES	HISTOPERMEABILITY FOR LIVE ANIMAL IMAGING	PHOTOSTABILITY	FLUOROGENESIS	REF.
Quinacrine	No (acidotropic stain, DNA stain)	Yes	Yes	No	65, 75-77
LysoTrackers	No (acidotropic stains)	Yes	No	No	9, 65, 77-79
Acridine orange	No (acidotropic stain, DNA/RNA stain)	Yes	Yes	No	65, 80-83
Dihydrorhodamine 123	No (ROS/RNS-dependent - also labels mitochondria)	No (<i>in vitro</i> only)	No	Yes (ROS-activated)	9, 84-87
Rhodamine-thiolactones	No (ROS-dependent)	Yes	Yes	Yes (ROS-reactive)	61, 88
Sudan Black B	Yes (lipids/MPO-dependent)	No (FA fixation <i>in vivo</i>)	NA (colorimetric stain)	NA (colorimetric stain)	5, 42, 89
Luminol	No (ROS-dependent, MPO-amplified)	No (<i>in vitro</i> only)	NA (chemoluminescent stain)	NA (chemoluminescent stain)	90
Tyramide-FITC / Cy3	Yes (MPO-reactive)	No (FA fixation <i>in vivo</i>)	No (FITC conjugate)	No	5, 91
			Yes (Cy3 conjugate)		

MUB ₄₀ / RI-MUB ₄₀ -Cy5	Yes (lactoferrin ligands)	No (peptides, FA fixation <i>in vitro</i> , <i>in vivo</i>)	Yes	No	60
NE680	Yes (elastase substrate)	No (peptide, MeOH fixation <i>ex vivo</i> , intranasal instillation in mouse)	Yes	Yes (enzyme-activated)	92
Elastase, cathepsin G, proteinases 3 and 4 substrates	Yes (enzyme substrates)	No (peptides, FA fixation <i>in vitro</i>)	Yes	Yes (enzyme-activated)	93
HAB	Yes (pH, ROS, MPO-independent fluorescence)	Yes (amphipathic small-molecule, log _{D7,4} = 2.21)	Yes (> 15 hrs under continuous 488 nm irradiation)	Yes (target protein-induced FTO)	Our study

Abbreviations: FA, formaldehyde; FITC, fluorescein isothiocyanate; FTO, Fluorescence Turn-On; MeOH, methanol; MPO, myeloperoxidase; NA, non-applicable; RNS, reactive nitrogen species; ROS, reactive oxygen species.

Methods

Compound synthesis, structural characterization and pKa prediction. Detailed synthetic procedures and analytical identification for compounds **2-8**, **10-12** and **14**, as well as pKa prediction for **HAB**, can be found in the Electronic Supporting Information.

Zebrafish. Transgenic and mutant stocks of zebrafish were raised and staged according to Westerfield.⁹⁴ AB wild-type fish and transgenic lines Tg(*mpx*:GFP)ⁱ¹¹⁴, Tg(*mpx*:GAL4.VP16)ⁱ²², Tg(Mfap4:mCherry-F) and Tg(UAS-E1b:nfsB.mCherry)^{c264} were used.³⁵⁻³⁷ Embryos were reared at 28 °C or 24 °C according to the desired speed of development. All timings in the text refer to the developmental stage at the reference temperature of 28.5 °C.⁹⁴ Embryo and larvae were anesthetized with 200 µg/ml tricaine (Sigma-Aldrich) during live *in vivo* imaging.

HAB labeling of live zebrafish embryo and larva.

Equilibrium protocol (Fig. 6, 9, S10 and S11, Video S5, S6 and S7): 72 hpf or 6 dpf zebrafish larvae, either wild-type AB specimens or transgenic specimens, were placed in individual wells (24-well culture plates; 10 embryos or larvae/well), incubated with **HAB** (10 µM in Volvic water from 10 mM stock solutions in DMSO) at room temperature for 1 hr in the dark, anaesthetized in buffered tricaine (Sigma) containing **HAB** (10 µM) then mounted in 35 mm glass-bottom dishes (Inagaki-Iwaki) in 1 % low-melting-point agarose containing **HAB** (10 µM) to ensure equilibrium conditions. The immobilized larvae were then covered with 2 ml Volvic water containing tricaine and **HAB** (10 µM) as described previously.⁴³ Negative controls consisted of Volvic water containing 0.1 % DMSO. For wild-type AB specimens as well as transgenic specimens, **HAB** was incubated for 1 hr.

Diffusion protocol (Fig. 5, 7, 8, Fig. S4, S9, Video S8): Wild-type AB zebrafish embryos and swimming larvae (24 hpf to 72hpf) were placed in individual wells (24-well culture plates; 10 embryos or larvae/well), incubated with **HAB** (10 µM in Volvic water from 10 mM stock solutions in DMSO) at room temperature for 1 hr in the dark, washed, anaesthetized in **HAB**-free buffered tricaine (Sigma) then mounted in 35 mm glass-bottom dishes (Inagaki-Iwaki) in **HAB**-free 1 % low-melting-point agarose. The immobilized larvae were then covered with 2 ml Volvic water containing tricaine as described previously.⁴³ Negative controls consisted of Volvic water containing 0.1 % DMSO. Practically, homogenous aqueous solutions of **HAB** were obtained by adding the drop of stock DMSO solutions on the inner wall of a plastic tube containing Volvic water at room temperature (20-23 °C), and vortexing without interruption for 20 s.

Sudan Black staining (Fig. 7). Embryos were fixed with 4% methanol-free formaldehyde (Poly-sciences, Warrington, PA) in phosphate-buffered saline (PBS) for 2 hours at room temperature, rinsed in PBS, incubated in Sudan Black (SB; Sigma-Aldrich) for 20 minutes, washed extensively in 70% ethanol in water, then progressively rehydrated in 0.1% Tween 20 in PBS as previously described.⁵

Zyosan microinjection in zebrafish larvae (Fig. 7). Zebrafish larvae (72 hpf) were anaesthetized by immersion in buffered tricaine immediately after the **HAB** labeling. They were injected with 1 nl of 0.4 x 10⁸/ml zyosan-Cy5 particles suspension using pulled borosilicate glass microcapillary (GC100F-15 Harvard apparatus) pipettes under a stereomicroscope (Stemi 2000, Carl Zeiss, Germany) with a mechanical micromanipulator (M-152; Narishige), and a Picospritzer III pneumatic microinjector (Parker Hannifin) set at a pressure of 20 psi and an injection time of 20 msec (subcutaneous injections) as previously described.⁴³

Competition experiments (Fig. 8). 72 hpf wild-type AB zebrafish larvae were placed into individual wells as previously described and co-incubated for 1 hr at room temperature with **HAB** (10 µM from a 10 mM stock solution in DMSO) and each competitor (100 µM from a 10 mM stock solution in DMSO) in Volvic water in the dark as previously described. Negative controls consisted of Volvic water containing 1.1 % DMSO. In this case, specimens were rapidly rinsed,

anaesthetized and mounted in **HAB**-free media for biological imaging. Practically, homogenous aqueous solutions of **HAB** +/- competitors were obtained by adding the drop of stock DMSO solutions on the inner wall of a plastic tube containing Volvic water at room temperature (20-23 °C), and vortexing without interruption for 20 s.

HAB labeling of live human neutrophils (Fig. 9 and S10). Peripheral human blood was collected from healthy patients at the ICAREB service of the Pasteur Institute (authorization DC No. 2008-68). All donors gave written informed consent in accordance with the Declaration of Helsinki principles. Blood was collected from the antecubital vein into tubes containing sodium citrate (3.8 % final) as anticoagulant. Human polymorphonuclear neutrophils were purified as described previously.⁹⁵ Briefly, plasma was removed by centrifugation (450 g, 15 min), and blood cells were resuspended in 0.9 % NaCl solution supplemented with 0.72 % Dextran. After red blood cells sedimentation, white blood cells were pelleted and further separated on a two layers Percoll (GE Healthcare) gradient (51-42 %) by centrifugation (240 g, 20 min). Peripheral Blood Mononuclear Cells (PBMC) (top layer) were isolated from polymorphonuclear neutrophils (bottom layer). Red blood cells were removed from the latter fraction using CD235a (glycophorin) microbeads (Miltenyi Biotec). Purified polymorphonuclear neutrophils were resuspended in the autologous plasma until experimental use. For **HAB** labeling, they were immediately put in RPMI 10 mM Hepes at 2×10^6 cells/ml. 1 ml of neutrophil suspension was distributed in 35 mm glass-bottom dishes and incubated at room temperature for 20 min for neutrophils adhesion. The medium was then replaced by the **HAB** staining solution (at 1, 5 or 10 μ M) in RPMI 10 mM Hepes; after 5-15 min at room temperature, **HAB**-labeled neutrophils were observed with a SP8 Leica confocal microscope, using a 63x water immersion objective. The 10 μ M **HAB** concentration gave the best results.

Live imaging, image processing and analysis. Confocal microscopy to detect **HAB** single labeling in wild-type zebrafish embryos and larvae was performed at 23-26 °C using a Leica SPE inverted microscope and a 16X oil immersion objective (PL FLUOTAR 16X/0.50 IMM). **HAB** was excited with a 488 nm laser and the fluorescence emission collected within the 550-650 nm range unless otherwise indicated. A Leica SP8 confocal microscope with a 20X oil immersion objective (HC PL APO CS2 20X/0.75 IMM) was used to live image transgenic larvae for colocalization studies and wt larvae for competition studies. Regarding **HAB**/mCherry acquisition, the following settings were applied: **HAB** (excitation 448 nm; emission 550-650 nm) and mCherry (excitation 552 nm; emission 660-750 nm) using a sequential acquisition mode. For GFP/**HAB** acquisition the following settings were applied: GFP (excitation 448 nm; emission 500-520 nm) and **HAB** (excitation 448 nm; emission > 600 nm). A 40X water immersion objective (HC PL APO CS2 40X / 1.1 water) was used also with the SP8 LEICA confocal microscope, to document at high resolution **HAB** labeling in neutrophils. For **HAB**-zymosan acquisition, the following settings were applied: **HAB** (excitation 488 nm; emission 491-601 nm) and Cy5-zymosan (excitation 638 nm; emission 683-795 nm). A 63x water immersion objective (HC PL APO CS2 63X / 1.2 water) was used to image **HAB** in live human neutrophils, following excitation at 448 nm and collecting the fluorescence emission in the 550-650 nm range. The 3D or 4D files generated by the confocal acquisitions were processed using the LAS-AF Leica software. Acquired Z-stacks (2 μ m serial optical sections for images taken using 16X and 20X objectives) were projected using maximum intensity projection and exported as AVI or TIFF files. Z stacks acquired with the 40X or 63X objectives (0.4 μ m to 1 μ m serial optical sections) were exported as AVI file. Frames were captured from the AVI files and handled with Powerpoint software to mount figures.

References

1. S. Masud, V. Torraca and A. H. Meijer, *Curr Top Dev Biol*, 2017, **124**, 277-329.
2. G. J. Lieschke, A. C. Oates, M. O. Crowhurst, A. C. Ward and J. E. Layton, *Blood*, 2001, **98**, 3087-3096.
3. D. Traver, P. Herbomel, E. E. Patton, R. D. Murphey, J. A. Yoder, G. W. Litman, A. Catic, C. T. Amemiya, L. I. Zon and N. S. Trede, *Advances in Immunology, Vol 81*, 2003, **81**, 253-330.
4. P. Herbomel, B. Thisse and C. Thisse, *Development*, 1999, **126**, 3735-3745.
5. D. Le Guyader, M. J. Redd, E. Colucci-Guyon, E. Murayama, K. Kissa, V. Briolat, E. Mordelet, A. Zapata, H. Shinomiya and P. Herbomel, *Blood*, 2008, **111**, 132-141.
6. K. M. Henry, C. A. Loynes, M. K. B. Whyte and S. A. Renshaw, *Journal of Leukocyte Biology*, 2013, **94**, 633-642.
7. E. A. Harvie and A. Huttenlocher, *Journal of Leukocyte Biology*, 2015, **98**, 523-537.
8. E. Suzuki, H. Kobayashi, Y. Kodama, T. Masujima and S. Terakawa, *Cell Motility and the Cytoskeleton*, 1997, **38**, 215-228.
9. C. F. Basso, N. Y. Li, K. Ragheb, G. Lawler, J. Sturgis and J. P. Robinson, *Cytometry Part B-Clinical Cytometry*, 2003, **51B**, 21-29.
10. R. Duval and C. Duplais, *Nat Prod Rep*, 2017, **34**, 161-193.
11. N. DiCesare and J. R. Lakowicz, *Tetrahedron Letters*, 2002, **43**, 2615-2618.
12. J. Prabhu, K. Velmurugan and R. Nandhakumar, *Spectrochim Acta A Mol Biomol Spectrosc*, 2015, **144**, 23-28.
13. C. G. Niu, A. L. Guan, G. M. Zeng, Y. G. Liu and Z. W. Li, *Analytica Chimica Acta*, 2006, **577**, 264-270.
14. S. C. Lee, N. Y. Kang, S. J. Park, S. W. Yun, Y. Chandran and Y. T. Chang, *Chem Commun (Camb)*, 2012, **48**, 6681-6683.
15. M. Tomasch, J. S. Schwed, L. Weizel and H. Stark, *Front Syst Neurosci*, 2012, **6**, 14.

16. B. Zhou, P. Jiang, J. Lu and C. Xing, *Arch Pharm (Weinheim)*, 2016, **349**, 539-552.
17. T. Fuchigami, Y. Yamashita, M. Haratake, M. Ono, S. Yoshida and M. Nakayama, *Bioorg Med Chem*, 2014, **22**, 2622-2628.
18. H. G. O. Alvim, E. L. Fagg, A. L. de Oliveira, H. C. B. de Oliveira, S. M. Freitas, M. A. E. Xavier, T. A. Soares, A. F. Gomes, F. C. Gozzo, W. A. Silva and B. A. D. Neto, *Organic & Biomolecular Chemistry*, 2013, **11**, 4764-4777.
19. A. Bessette, T. Auvray, D. Desilets and G. S. Hanan, *Dalton Transactions*, 2016, **45**, 7589-7604.
20. P. M. Alexander, H, *Nature*, 1962, **194**, 2.
21. D. Kulms and T. Schwarz, *Skin Pharmacology and Applied Skin Physiology*, 2002, **15**, 342-347.
22. S. J. Lord, H. L. Lee, R. Samuel, R. Weber, N. Liu, N. R. Conley, M. A. Thompson, R. J. Twieg and W. E. Moerner, *J Phys Chem B*, 2010, **114**, 14157-14167.
23. S. D. Barker, K. Wilson and R. K. Norris, *Australian Journal of Chemistry*, 1995, **48**, 1969-1979.
24. P. G. E. Alcorn, Wells, P. R., *Australian Journal of Chemistry*, 1965, **18**, 1377-1389.
25. V. Balasubramaniyan, *Chemical Reviews*, 1966, **66**, 567-+.
26. D. Skalamera, L. P. Cao, L. Isaacs, R. Glaser and K. Mlinaric-Majerski, *Tetrahedron*, 2016, **72**, 1541-1546.
27. A. Niemann, J. Baltés and H. P. Elsasser, *Journal of Histochemistry & Cytochemistry*, 2001, **49**, 177-185.
28. X. J. Yang, C. M. Shi, R. Tong, W. P. Qian, H. E. Zhou, R. X. Wang, G. D. Zhu, J. J. Cheng, V. W. Yang, T. M. Cheng, M. Henary, L. Strekowski and L. W. K. Chung, *Clinical Cancer Research*, 2010, **16**, 2833-2844.
29. R. A. Duval, R. L. Allmon and J. R. Lever, *J Med Chem*, 2007, **50**, 2144-2156.
30. P. Boeck, C. A. B. Falcao, P. C. Leal, R. A. Yunes, V. Cechinel, E. C. Torres-Santos and B. Rossi-Bergmann, *Bioorganic & Medicinal Chemistry*, 2006, **14**, 1538-1545.
31. X. L. Zi and A. R. Simoneau, *Cancer Research*, 2005, **65**, 3479-3486.
32. M. J. Waring, *Bioorg Med Chem Lett*, 2009, **19**, 2844-2851.
33. I. Ziegler, T. McDonald, C. Hesslinger, I. Pelletier and P. Boyle, *J Biol Chem*, 2000, **275**, 18926-18932.
34. C. W. Higdon, R. D. Mitra and S. L. Johnson, *PLoS One*, 2013, **8**, e67801.
35. Q. T. Phan, T. Sipka, C. Gonzalez, J. P. Levraud, G. Lutfalla and N. C. Mai, *Plos Pathog*, 2018, **14**.
36. F. Ellett, L. Pase, J. W. Hayman, A. Andrianopoulos and G. J. Lieschke, *Blood*, 2011, **117**, E49-E56.
37. S. A. Renshaw, C. A. Loynes, D. M. I. Trushell, S. Elworthy, P. W. Ingham and M. K. B. Whyte, *Blood*, 2006, **108**, 3976-3978.
38. M. O. Crowhurst, J. E. Layton and G. J. Lieschke, *Int J Dev Biol*, 2002, **46**, 483-492.
39. C. T. Pham, *Nat Rev Immunol*, 2006, **6**, 541-550.
40. K. Wang, X. Fang, N. Ma, Q. Lin, Z. Huang, W. Liu, M. Xu, X. Chen, W. Zhang and Y. Zhang, *Fish Shellfish Immunol*, 2015, **44**, 109-116.
41. B. J. Bain, *Am J Hematol*, 2010, **85**, 707.
42. W. van den Ancker, T. M. Westers, D. C. de Leeuw, Y. F. van der Veeke, A. Loonen, E. van Beckhoven, G. J. Ossenkoppele and A. A. van de Loosdrecht, *Cytometry B Clin Cytom*, 2013, **84**, 114-118.
43. E. Colucci-Guyon, J. Y. Tinevez, S. A. Renshaw and P. Herbomel, *J Cell Sci*, 2011, **124**, 3053-3059.
44. E. K. Macrae and K. B. Pryzwansky, *Carlsberg Research Communications*, 1984, **49**, 315-322.
45. P. M. Elks, M. van der Vaart, V. van Hensbergen, E. Schutz, M. J. Redd, E. Murayama, H. P. Spaink and A. H. Meijer, *PLoS One*, 2014, **9**, e100928.
46. Y. H. Chen, W. H. Wang, Y. H. Wang, Z. Y. Lin, C. C. Wen and C. Y. Chern, *Molecules*, 2013, **18**, 2052-2060.
47. B. P. Bandgar, S. A. Patil, R. N. Gacche, B. L. Korbadi, B. S. Hote, S. N. Kinkar and S. S. Jalde, *Bioorganic & Medicinal Chemistry Letters*, 2010, **20**, 730-733.
48. J. Z. Wu, J. L. Li, Y. P. Cai, Y. Pan, F. Q. Ye, Y. L. Zhang, Y. J. Zhao, S. L. Yang, X. K. Li and G. Liang, *Journal of Medicinal Chemistry*, 2011, **54**, 8110-8123.
49. D. J. Kwon, S. M. Ju, G. S. Youn, S. Y. Choi and J. Park, *Food and Chemical Toxicology*, 2013, **58**, 479-486.
50. N. Wu, J. Liu, X. Z. Zhao, Z. Y. Yan, B. Jiang, L. J. Wang, S. S. Cao, D. Y. Shi and X. K. Lin, *Tumor Biology*, 2015, **36**, 9667-9676.
51. S. Hatzieremia, A. I. Gray, V. A. Ferro, A. Paul and R. Plevin, *British Journal of Pharmacology*, 2006, **149**, 188-198.
52. M. Hachet-Haas, K. Balabanian, F. Rohmer, F. Pons, C. Franchet, S. Lecat, K. Y. C. Chow, R. Dagher, P. Gizzi, B. Didier, B. Lagane, E. Kellenberger, D. Bonnet, F. Baleux, J. Haiech, M. Parmentier, N. Frossard, F. Arenzana-Seisdedos, M. Hibert and J. L. Galzi, *Journal of Biological Chemistry*, 2008, **283**, 23189-23199.
53. F. de Campos-Buzzi, J. P. de Campos, P. P. Tonini, R. Correa, R. A. Yunes, P. Boeck and V. Cechinel-Filho, *Archiv Der Pharmazie*, 2006, **339**, 361-365.
54. M. S. Cooper, L. A. D'Amico and C. A. Henry, *Methods Cell Biol*, 1999, **59**, 179-204.

55. E. Murayama, M. Sarris, M. Redd, D. Le Guyader, C. Vivier, W. Horsley, N. Trede and P. Herbomel, *Nature Communications*, 2015, **6**.
56. D. Dalle Nogare, K. Somers, S. Rao, M. Matsuda, M. Reichman-Fried, E. Raz and A. B. Chitnis, *Development*, 2014, **141**, 3188-3196.
57. N. Yakuwa, T. Inoue, T. Watanabe, K. Takahashi and F. Sendo, *Microbiol Immunol*, 1989, **33**, 843-852.
58. K. Ley, H. M. Hoffman, P. Kubers, M. A. Cassatella, A. Zychlinsky, C. C. Hedrick and S. D. Catz, *Sci Immunol*, 2018, **3**.
59. J. L. Eyles, A. W. Roberts, D. Metcalf and I. P. Wicks, *Nat Clin Pract Rheum*, 2006, **2**, 500-510.
60. M. C. Anderson, T. Chaze, Y. M. Coic, L. Injarabian, F. Jonsson, N. Lombion, D. Selimoglu-Buet, J. Souphron, C. Ridley, P. Vonaesch, B. Baron, E. T. Arena, J. Y. Tinevez, G. Nigro, K. Nothelfer, E. Solary, V. Lapierre, T. Lazure, M. Matondo, D. Thornton, P. J. Sansonetti, F. Baleux and B. S. Marteyn, *Cell Chem Biol*, 2018, **25**, 483-493 e489.
61. X. Chen, K. A. Lee, E. M. Ha, K. M. Lee, Y. Y. Seo, H. K. Choi, H. N. Kim, M. J. Kim, C. S. Cho, S. Y. Lee, W. J. Lee and J. Yoon, *Chem Commun (Camb)*, 2011, **47**, 4373-4375.
62. D. D. Li, N. Ropert, A. Koulakoff, C. Giaume and M. Oheim, *Journal of Neuroscience*, 2008, **28**, 7648-7658.
63. B. Lemieux, M. D. Percival and J. P. Falgueyret, *Analytical Biochemistry*, 2004, **327**, 247-251.
64. T. Sasaki, S. S. Lian, J. Qi, P. E. Bayliss, C. E. Carr, J. L. Johnson, S. Guha, P. Kobler, S. D. Catz, M. Gill, K. L. Jia, D. J. Klionsky and S. Kishi, *Plos Genetics*, 2014, **10**.
65. A. Pierzynska-Mach, P. A. Janowski and J. W. Dobrucki, *Cytometry Part A*, 2014, **85A**, 729-737.
66. M. Wu, T. Baumgart, S. Hammond, D. Holowka and B. Baird, *J Cell Sci*, 2007, **120**, 3147-3154.
67. H. Y. Chen, D. M. Chiang, Z. J. Lin, C. C. Hsieh, G. C. Yin, I. C. Weng, P. Guttermann, S. Werner, K. Henzler, G. Schneider, L. J. Lai and F. T. Liu, *Sci Rep*, 2016, **6**, 34879.
68. A. W. Segal, *Annual Review of Immunology*, 2005, **23**, 197-223.
69. M. A. Kolber and P. A. Henkart, *Biochimica Et Biophysica Acta*, 1988, **939**, 459-466.
70. J. P. Crow, *Nitric Oxide-Biology and Chemistry*, 1997, **1**, 145-157.
71. Y. Qin, M. Lu and X. G. Gong, *Cell Biology International*, 2008, **32**, 224-228.
72. L. Yuan, L. Wang, B. K. Agrawalla, S. J. Park, H. Zhu, B. Sivaraman, J. Peng, Q. H. Xu and Y. T. Chang, *J Am Chem Soc*, 2015, **137**, 5930-5938.
73. A. Budnjo, S. Narawane, C. Grauffel, A. S. Schillinger, T. Fossen, N. Reuter and B. E. Haug, *J Med Chem*, 2014, **57**, 9396-9408.
74. W. C. Groutas, D. Dou and K. R. Alliston, *Expert Opin Ther Pat*, 2011, **21**, 339-354.
75. A. Parks, X. Charest-Morin, M. Boivin-Welch, J. Bouthillier and F. Marceau, *PeerJ*, 2015, **3**, e1314.
76. A. T. Sumner, *Histochemistry*, 1986, **84**, 566-574.
77. P. Huang, Y. Zou, X. Z. Zhong, Q. Cao, K. Zhao, M. X. Zhu, R. Murrell-Lagnado and X. P. Dong, *J Biol Chem*, 2014, **289**, 17658-17667.
78. T. Sasaki, S. Lian, J. Qi, P. E. Bayliss, C. E. Carr, J. L. Johnson, S. Guha, P. Kobler, S. D. Catz, M. Gill, K. Jia, D. J. Klionsky and S. Kishi, *PLoS Genet*, 2014, **10**, e1004409.
79. E. Dona, J. D. Barry, G. Valentin, C. Quirin, A. Khmelinskii, A. Kunze, S. Durdu, L. R. Newton, A. Fernandez-Minan, W. Huber, M. Knop and D. Gilmour, *Nature*, 2013, **503**, 285-289.
80. I. Vermes and C. Haanen, *Adv Clin Chem*, 1994, **31**, 177-246.
81. J. A. Udovich, D. G. Besselsen and A. F. Gmitro, *J Microsc*, 2009, **234**, 124-129.
82. T. J. van Ham, J. Mapes, D. Kokel and R. T. Peterson, *FASEB J*, 2010, **24**, 4336-4342.
83. B. Tucker and M. Lardelli, *Zebrafish*, 2007, **4**, 113-116.
84. M. Poot, Y. Z. Zhang, J. A. Kramer, K. S. Wells, L. J. Jones, D. K. Hanzel, A. G. Lugade, V. L. Singer and R. P. Haugland, *J Histochem Cytochem*, 1996, **44**, 1363-1372.
85. X. Wang, H. Fang, Z. Huang, W. Shang, T. Hou, A. Cheng and H. Cheng, *J Mol Med (Berl)*, 2013, **91**, 917-927.
86. I. D. Trayner, A. P. Rayner, G. E. Freeman and F. Farzaneh, *J Immunol Methods*, 1995, **186**, 275-284.
87. J. P. Crow, *Nitric Oxide*, 1997, **1**, 145-157.
88. Y. Koide, Y. Urano, K. Hanaoka, T. Terai and T. Nagano, *J Am Chem Soc*, 2011, **133**, 5680-5682.
89. B. J. Bain, in *Dacie and Lewis Practical Haematology (Twelfth Edition)*, ed. B. J. Bain, Bates, I., Laffan, M. A., Elsevier, 2017.
90. S. Bedouhene, F. Moulti-Mati, M. Hurtado-Nedelec, P. M. Dang and J. El-Benna, *Am J Blood Res*, 2017, **7**, 41-48.
91. G. Lauter, I. Soll and G. Hauptmann, *Methods Mol Biol*, 2014, **1082**, 175-185.
92. S. Kossodo, J. Zhang, K. Groves, G. J. Cuneo, E. Handy, J. Morin, J. Delaney, W. Yared, M. Rajopadhye and J. D. Peterson, *Int J Mol Imaging*, 2011, **2011**, 581406.

93. P. Kasperkiewicz, Y. Altman, M. D'Angelo, G. S. Salvesen and M. Drag, *J Am Chem Soc*, 2017, **139**, 10115-10125.
94. M. Westerfield, *The Zebrafish Book. A Guide for the Laboratory Use of Zebrafish (Danio rerio)*, University of Oregon Press, 1995.
95. V. Monceaux, C. Chiche-Lapierre, C. Chaput, V. Witko-Sarsat, M. C. Prevost, C. T. Taylor, M. N. Ungeheuer, P. J. Sansonetti and B. S. Marteyn, *Blood*, 2016, **128**, 993-1002.

Acknowledgements

The authors wish to acknowledge the following contributors: Dr. L. Bianchi and Prof. G. Petrillo for the generous gift of a reference of compound **10**; Dr. P. Leal for the gift of xanthoxylone; Prof. S. Renshaw and Prof. G. Lutfalla for providing with the zebrafish transgenic Tg(*mpx*:GAL4.VP16)ⁱ²² and Tg(*mfap4*:mCherryF) lines, respectively; Dr. F. Niedergang for the gift of cy5-zymosan; T. M. R. Gianeti and Dr. A. Maciuk for their practical help regarding NIR fluorescence and HRMS analysis, respectively; A. Blin for taking pictures of UVA-irradiated cuvettes in Fig. 4; Dr. N. Bizat for preliminary labelling experiments in *C. elegans*; V. Briolat, Y. Rolin and N. Aimar for fish husbandry, as well as L. Boucontet for helping with zebrafish embryo preparation; Dr. M. Anderson for the preparation of isolated human neutrophils; Dr. A. Cras for fruitful discussions regarding the biology of human blood cells. R. Duval gratefully acknowledges Prof. R. J. Nunes, Prof. B. Rossi-Bergmann and Prof. N. Leulliot for permitting certain experiments to be conducted in their laboratories. The Conselho Nacional de Desenvolvimento Científico e Tecnológico (CNPq) and the Pasteur Institute are acknowledged for financial support, as well as J. Moreira for helping with the production of the grant scientific proposal in Portuguese.

Notes and references

The abbreviations used in the present article as well as in the ESI are: AcOEt, ethyle acetate; AcOH, acetic acid; BF, bright field; CC, column chromatography; CHCl₃, chloroform; DHR, dihydrorhodamine; DIC, Differential Interference Contrast; DMF, dimethylformamide; DMSO, dimethylsulfoxide; DPP, *N*-dansyl-*N'*-phenylpiperazine; FACS, fluorescence-activated cell sorting; F, fluorescence quantum yield; HAB, 4'-hydroxy-3-aminobenzochalcone; HRMS, high-resolution mass spectra; ICG, indocyanine green; LTR, LysoTrackerRed; MeCN, acetonitrile; MPO, myeloperoxidase; PBMC, peripheral blood mononuclear cells; ROS, reactive oxygen species; RTL, rhodamine-thiolactone; QA, quinacrine; SB, Sudan Black.

Keywords: benzochalcone • histopermeability • fluorogenesis • zebrafish • neutrophils • granules • live imaging

Author contributions

E. C.-G. designed, performed and analysed the **HAB**-zebrafish experiments and contributed to the writing of the manuscript. A. S. B. and S. D. S. O. performed **HAB** phenotypic screening. M. B. and I. C. B. performed the fluorescence spectroscopy experiments. B. S. M. provided with human neutrophils and PBMC. K. L. performed the HRMS analysis. P. H. assisted with helpful discussion and participated in the writing of the manuscript. R. D. designed **HAB**, performed the synthesis and structural analysis of all compounds, performed log_{D7,4} measurements, co-analysed all biological experiments, and wrote the manuscript.

Additional information

Electronic Supplementary Information (ESI) such as detailed experimental procedures regarding compound synthesis, structural and spectral characterization, pK_a prediction, bioimaging experiments, staining dynamics of **HAB** in 72 hpf zebrafish larvae (videos) and complementary figures, accompanies this article at <http://rsc.org/chemicalscience>.

Competing financial interests: the authors declare no competing financial interests.

How to cite this article: